UNIVERSITY OF CALIFORNIA,
IRVINE

EEG and spiking relationship under anesthesia

THESIS

submitted in partial satisfaction of the requirements
for the degree of

MASTER OF SCIENCE
in Biomedical Engineering

by

Marta Alcalá Álvarez

Thesis Committee:

Professor Zoran Nenadic, Chair
Professor Gregory J. Brewer
Professor Beth A. Lopour

2016

CONTENTS

LIST OF FIGURES

LIST OF TABLES

LIST OF EQUATIONS

ACKNOWLEDGEMENTS

Firstly, this thesis is only possible thanks to the support of the Balsells Fellowship throughout my studies at UC Irvine and the National Science Foundation for funding the project. I am truly grateful for this opportunity, especially to Mr. Peter Balsells and Prof. Roger Rangel.

Secondly, I would like to thank my advisor Prof. Zoran Nenadic for his implication in the project and his expertise that helped elevate the quality of this work as well as Prof. Yama Akbari and his lab for allowing us to participate in their experiments and filling in our biology blanks.

I am also thankful to my lab mates for sharing their knowledge and code, particularly to Agnieszka Szymanska, who had a major role in the development of this thesis. I am happy to have gotten the chance to work on this project and I appreciate her guidance and support along with the food adventures.

Last but not least, thanks to the committee members Prof. Gregory Brewer and Prof. Beth Lopour for taking the time to read and review this thesis.

ABSTRACT OF THE THESIS

EEG and spiking relationship under anesthesia

By

Marta Alcalá Álvarez

Master of Science in Biomedical Engineering

University of California, Irvine, 2016

Professor Zoran Nenadic, Chair

The behavior of the brain under general anesthesia remains poorly understood despite the widespread use of anesthesia in medical practice, especially from the electrophysiological standpoint. This thesis studies the relationship between electroencephalographic signals (EEG) and extracellular recordings in the cortex of a rat under different concentrations of isoflurane anesthesia causing burst suppression pattern. EEG signals were recorded from two screw electrodes placed directly on the surface of the brain. The extracellular recordings from which local field potentials (LFPs) and multi-unit activity (MUA) were extracted were recorded from a 7-channel depth electrode. Correlation between different frequency bands of the EEG and firing rate of the recorded neuronal population was assessed at different cortical depths, with the highest correlations being in the theta and high gamma bands. Only 770 out of the 45,121 detected spikes occurred while the EEG was isoelectric, making the EEG bursting a good predictor of the spiking activity. Spike-triggered average and impulse response analysis on both the EEG and LFP signals showed a significant response at the time of the action potential. As anesthesia was increased, the response became stronger, suggesting that functional connectivity, even across hemispheres, is enhanced under isoflurane.

CHAPTER 1

Introduction

1.1. Motivation

Anesthesia is a vital component of medical practice. Although the number of minimally invasive surgeries is steadily increasing, general anesthesia – from now on referred as anesthesia – remains a clinical necessity in many surgical procedures, especially those with life-saving outcomes. While the first surgical procedure using anesthesia was performed more than 170 years ago [1], the effects of anesthesia, especially on the brain, are still not completely understood [2]. The abundance of anesthetics – each with its own dosage, induction mechanism, and way of injection – is one of the many factors that makes the study of anesthesia so complex. Monitoring the level of anesthesia is also extremely challenging since it affects each individual differently, making it difficult to infer population effects. It has been proven that as the level of anesthesia deepens, conventional spectrally-based parameters that correctly predict loss and recovery of consciousness [3] no longer reflect properly the level of anesthesia [4]. At such deep levels, anesthesia induces a pattern in the electroencephalographic signals called burst suppression pattern. This pattern is actually similar to certain pathological patterns such as periodic lateralizing epileptiform discharges or paroxysmal bursts caused by the inhibition of glutamate transporters [5]. In fact, some electroencephalographic patterns have been shown to be useful predictors of

outcome in status epilepticus [6] and suppression bursts are indicative of an unfavorable outcome for comatose patients after cardiorespiratory arrest [7].

Thus, studying the burst suppression pattern caused by anesthesia not only at a cortical level but also at a neuronal level could provide a valuable insight into how neuronal connections adjust under such conditions and may as well be of use to the pathologies mentioned above. Studies of electrophysiological events under anesthesia at multiple scales are rare and not usually conducted at a high enough level of anesthesia to produce burst suppression pattern.

1.2. Background

1.2.1. Electrocorticography

Electrocorticography (ECoG) is the recording of the electrical activity of the brain directly on its surface by means of electrodes placed below the skull, either subdurally or epidurally. Compared to scalp electroencephalography (EEG), EcoG has a much higher signal-to-noise ratio (normally 5 to 10 times higher than that of EEG), and temporal and spatial resolution (tenths of millimeters versus centimeters [8]). In addition, it is not as susceptible to electrooculographic and electromyographic artifacts, and has a broader bandwidth (0-200 Hz versus 0-40 Hz [8]) [9]. In this thesis, EcoG signals will be referred to as EEG since we are using screw electrodes that drill into the skull and sit on top of the dura instead of traditional subdurally implanted ECoG grids.

1.2.2. Extracellular recordings

Extracellular recordings are an electrophysiological method to record the electrical potential from outside the cells, conventionally with a depth microelectrode. Extracellular recordings are usually separated by frequency range because, as stated by [10], “an extracellular electrode records slow events that originate from a large number of neighboring neurons, whereas the action potentials are recorded only for the cell(s) immediately adjacent to the electrode.”

This distinction gives rise to two distinct types of signals: Local Field Potentials (LFPs) and Multi-Unit Activity (MUA). Both are recorded from the same microelectrode but are filtered to retain either the low (LFPs) or high (MUA) frequencies.

Regarding LFPs, the spatial spread is not well defined, and studies investigating this topic present contradictory results. Whereas [11], [12] report that LFPs reflect extremely local activity – that of a region of approximately 250 μm around the microelectrode tip – other studies establish an influence area on the millimeter scale [13],[14]. Some of the known mechanisms that contribute to extracellular fields are the following: synaptic activity, fast action potentials, calcium potentials, intrinsic currents and resonances, spike afterhyperpolarizations and ‘down’ states, gap junctions and neuron-glia interactions, and ephaptic effects [15].

As for MUA, the high frequencies of the extracellular recordings contain the action potentials (AP). An action potential or spike is a rapid and pronounced change in the axon’s membrane polarity. It lasts for approximately 1 ms. During the course of an action potential, the voltage across the membrane is at first inverted: due to the entrance of sodium ions inside the cell, the interior of the cell gets positive relative to the outside. This is called depolarization of the cell. Then, the sodium channels close and the potassium ones open, allowing potassium ions to leave the cell and causing the repolarization of the cell, i.e. the cell interior goes back to being negative with respect to the outside. The firing of action potentials is an all-or-none response, and it happens when a

certain threshold in reached (typically, around -55 mV, reaching 40 mV at the peak depolarization, and being -70 mV the resting potential). Extracellularly-recorded APs can have many different waveforms depending on the microelectrode position relative to the cell [16].

1.2.3. Known effects of general anesthesia

Stating the effects of anesthesia is challenging due to the existence of many types of anesthetic drugs with different induction mechanisms and targets. In general, anesthetics produce unconsciousness, immobility, amnesia, and analgesia by decreasing the cortical activity of the brain. This inhibitory effect on cortical activity appears on the electroencephalographic signals as shifts from low amplitude and high frequency to high amplitude and low frequency, and also produces waveforms typical of sleep stages [17]. These changes reflect the alteration that neurons undergo due to anesthesia: anesthetics either increase membrane responsiveness to inhibitors or decrease excitability, causing hyperpolarization of the neurons [2], [18]. This alteration of the neurotransmission is the cause of unconsciousness [19] and can be induced in different ways depending on the anesthetic drug (see Table 1).

Table 1. Ionic mechanisms and targets of current clinical anesthetics. Abbreviations: Ach, acetylcholine; AMPA, α-amino-3-hydroxy-5-methyl-4-isoxazolepropionic acid; $GABA_A$, type A γ-aminobutyric acid; NMDA, N-methyl-D-aspartate. From [2]. Reprinted with permission from AAAS.

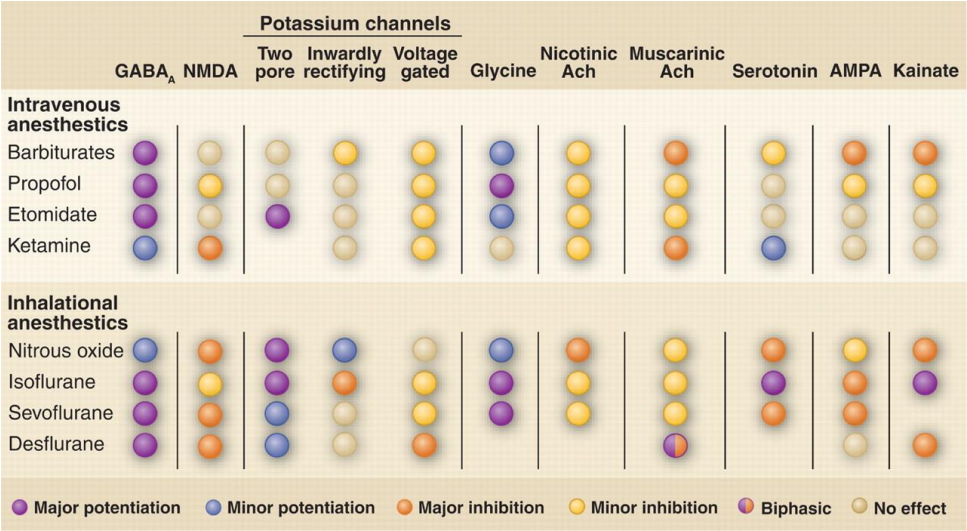

Isoflurane is an inhalational anesthetic widely used in veterinary anesthesia and experimental procedures on animals. Isoflurane induces in neurons "a hyperpolarization and increased membrane conductance in a reversible and concentration-dependent manner" [18] and also "enhances fast synaptic inhibition in the brain mediated by $GABA_A$ receptors" [20].

The effects of anesthesia are also greatly dependent on the individual, making the comparison of data from different individuals difficult to accomplish, even under the same experimental conditions. Weight, for example, is the most straightforward factor that influences the effects produced by anesthesia, so that dosing guidelines are often specified per kilogram [21].

The dose of administered anesthetic determines the effects seen in the EEG signals. After induction, at low concentrations of the anesthetic drug, there is a decrease in the beta activity (12–30 Hz) and an increase in the alpha (8–12 Hz) and delta (1–4 Hz) activity [19]. As the concentration of anesthetic increases, a burst suppression phase is reached. This pattern is characterized by a predominant quiescence interrupted by periods of high-amplitude activity, i.e. bursts (see Figure 3C for an example). The burst suppression phase is one of the anesthesia-induced EEG phases appropriate for surgical procedures [19].

Time under anesthesia is also a very important factor to consider when dealing with different concentrations of anesthesia; having a rat under a low level of anesthesia for a long time may have equivalent effects on the EEG as having the rat under a higher level for a shorter period of time [22].

1.3. Objective of Present Study

The general aim of this study is to determine the relationship between cortical brain signals and extracellular potentials during anesthesia-induced burst suppression, and the changes that this relationship undergoes as a result of the increase in the anesthesia concentration.

In this context, this thesis seeks to answer the following questions:

- How related are EEG and extracellular signals?
- How does the reduced cortical activity as established by the EEG translate at a neuronal level?

CHAPTER 2

Materials and Methods

2.1. Experimental procedure

The neurophysiological data used was recorded from a Wistar rat undergoing surgery for the implantation of four permanent EEG screw electrodes in the skull.

The experimental procedure for the surgery was the following. First, the rat was introduced into an induction chamber with a 5% isoflurane flow. Once the rat was unresponsive, it was mounted in a stereotactic frame. Isoflurane was then administered at a 2% concentration through a nose cone. In order to keep the position of the rat's head still throughout the surgery, the head was fixed with ear bars. A rectal probe was used to monitor body temperature and an electromyography sensor was placed on a paw to detect movement that could interfere with the brain signals. The head was then shaved and disinfected, preparing it for the incision. The first incision was made in the back of the head. Suture thread was used to keep the scalp apart, allowing the surgeon to inspect the surface of the skull. Burr hole positions were set relative to bregma, the intersection point between the frontal bone and the parietal bones. Therefore, the surgeon had to find this anatomical landmark before proceeding with the surgery. After finding bregma, the coordinates for the electrodes were marked (see Figure 1) and the burr holes were

drilled. Finally, the two EEG electrodes and the depth microelectrode were inserted into their respective burr holes. Ventilation rate was checked throughout the experiments by counting the number of breaths per minute as well as observing paw color to make sure that the animal did not show signs of hypoxia which could alter the brain signals.

The setting described above was the basis for the experiments. As shown in Figure 1, the depth microelectrode was placed in position B, EEG channel 1 in position A and EEG channel 2 in position C. Electrodes in A and B were located in the primary motor cortex (M1), and electrode in C was located in the primary somatosensory cortex hindlimb region (S1HL), according to [23].

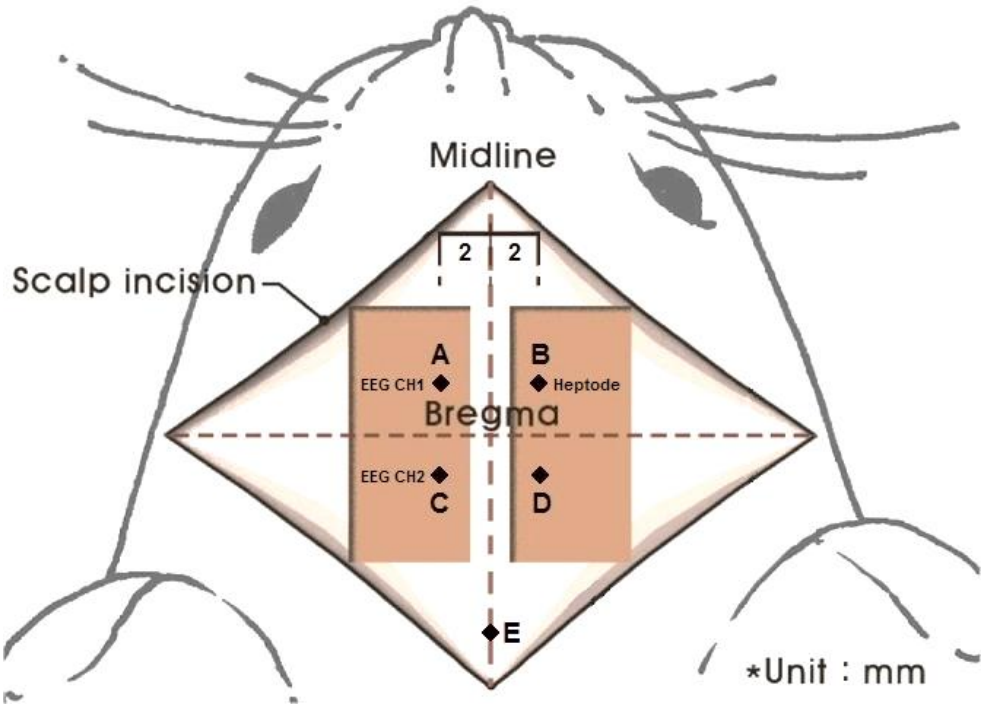

Figure 1. Electrode placement on the surface of the brain of the rat. Positions A to D are set ± 2 mm in relation to bregma. The depth microelectrode in B is referenced to a screw electrode at D. EEG electrodes are located at A and C and are referenced at the cerebellum (E). Adapted from [24].

2.2. Data acquisition

The depth electrode was a 7 core quartz-platinum/tungsten microelectrode (Thomas RECORDING GmbH). The measured impedances for the heptode prior to the experiment were the following for each of the channels: 0.27, 0.20, 0.28, 0.25, 0.26, 0.19 and 0.20 MΩ. The use of a multisensor electrode compared to a single-sensor electrode has proven to be more reliable to isolate multiple single units in the cortex using a single probe [25].

Extracellular recordings were sampled at a frequency of 25 kHz and EEG at 1.5 kHz.

We conducted two different experiments. We first varied the depth of the extracellular microelectrode to determine how related the EEG and the spikes were. In a second experiment, we varied the concentration of the anesthetic to see the effects that the increase in isoflurane concentration had on individual neurons and on the EEG-spiking relationship, using the first experiment as the baseline.

- **Baseline experiment**

Isoflurane was set at 1.5%. The heptode was lowered 1710 μm below the surface of the skull through the burr hole and into the cortex. We simultaneously recorded approximately four minutes of EEG and extracellular signals at 8 different heptode depths – P1 to P8 –, starting at 1710 μm and advancing the position 10 μm every time to reach 1780 μm.

- **Isoflurane variation experiment**

The heptode position was fixed at 1780 μm below the skull. The isoflurane concentration was set at 1.5% and was increased in 1% increments until reaching 3.5%. We simultaneously recorded two approximately two-minute EEG and extracellular signals at 1.5% and one at 2.5% and 3.5% isoflurane.

Time stamps were generated at the time of each data point acquisition for both EEG and extracellular recordings and were used to synchronize the two signals.

At the start of the isoflurane variation experiment, the rat had been under anesthesia for over two hours. This means that the percentage of anesthesia being administered to the rat is no longer necessarily a good indicator of the depth of anesthesia and another quantitative measure such as burst suppression ratio may be more appropriate. The burst suppression ratio (1) is widely used in anesthesia studies [4], [26], [27] and provides an electrophysiologically objective measure of the depth of anesthesia by quantifying the percentage of time that the EEG is isoelectric.

$$BSR(\%) = \frac{total\ time\ of\ suppression}{total\ time\ of\ the\ signal} \cdot 100 \quad (1)$$

2.3. Preprocessing

Extracellular recordings were processed in two ways to obtain local field potentials (LFP) and multi-unit activity (MUA). In order to obtain the LFPs, recordings were bandpass filtered from 1 to 300 Hz using a 4th order Butterworth filter. Sixty Hertz noise was reduced with a 1st order FFT notch filter. In order to obtain the MUA, extracellular recordings were firmware filtered (band pass, from 300 to 3,000 Hz). To avoid the residual 60 Hz noise, MUA were further high-pass filtered at 100 Hz with a 1st order FFT filter.

Regarding the EEG, initial correlation analysis was performed with the raw data filtered only for eliminating the power-line noise at 60 Hz with a 4th order Butterworth filter. For further analysis, EEG was also band passed from 2.5 to 110 Hz. The filter cut-off frequencies were determined based on the MUA firing frequencies of the baseline experiment since the MUA firing frequencies dictated the highest frequencies that we were interested in. More than 97% of the MUA firing frequencies were below 110 Hz (see Figure 2).

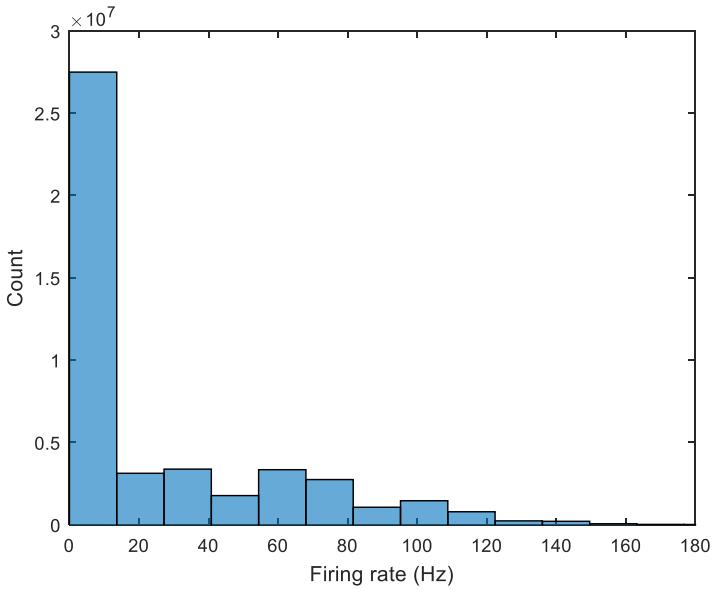

Figure 2. Histogram of the MUA firing frequencies in 1.5% isoflurane.

All the data processing and analysis was performed in MATLAB using custom-made programs.

2.4. Data Analysis

2.4.1. Detection and Sorting

The detection of the spikes was performed using the matched filters described in [28]. Essentially, a manual selection of 20 extracellular action potentials and 20 noise samples – taken from a single 1.5% isoflurane recording – allows generating a matched template for action potentials and a noise covariance matrix, assuming spatially white noise. An action potential is detected if the output of the filter is greater than a set threshold. In this case, we used a threshold of five standard deviations above the noise median for the baseline experiment and four standard deviations

above the noise median for the isoflurane variation experiment. Both thresholds were chosen empirically after visual inspection of the detected spikes. At the optimal threshold, the detector had an 84.62% and a 16.63% average true positive and false positive rate, respectively, when tested on tetrode data from a locust antennal lobe [28]. With a lower threshold, the number of false positives increases and the quality and isolation of the action potentials decreases. Increasing the threshold, on the other hand, brings the risk of missing too many spikes and does not prevent the detection of overlapping spikes either. The performance of the detector is a major factor in the accuracy of the calculations described in following sections since all of them are based on spike detection.

After detection, spike sorting – i.e. grouping of the spikes based on their neuron of origin – is another crucial task when trying to derive information about neural networks. Spike sorting presents several challenges mainly due to the nature of the data. Background noise, either biological or electrical, and overlapping spikes from different neurons make the correspondence between spikes and neurons quite difficult. A number of classification methods have been proposed to sort action potentials, such as: principal component analysis, cluster analysis, and Bayesian clustering [29]. In this thesis, source location was used as the feature for the classification of the multi-sensor extracellular action potentials, in a slightly modified version of the technique described in [30]. Electrode impedance was introduced in the feature extraction model, and a Parzen window density based clustering algorithm was used instead of expectation maximization. Each dataset was sorted independently with the same sensor location, average spike duration and electrode impedance parameters.

2.4.2. Firing rate

Firing rate was determined by counting the number of detected spikes in a 120 ms sliding window, i.e. the firing rate is the number of spikes that were detected in the 60 ms before and after a given time point. The selection of the window size was made based on the average duration of an EEG oscillation within a burst, but the firing rate was also calculated for window sizes ranging from 100 to 150 ms with no significant differences in either the firing rate results or in the correlation between EEG and firing rate explained below.

2.4.3. Cross-Correlation

For two discrete time-series, cross-correlation is defined as (2), where r_{xy} is the correlation coefficient for each of the lags l between the two signals x and y.

$$r_{xy}(l) = \sum_{n=-\infty}^{\infty} x(n) \cdot y(n-l), \qquad l = 0, \pm 1, \pm 2, \ldots \tag{2}$$

Cross-correlation is a measure of how similar two signals are as a function of the delay between them.

Cross-correlation coefficients can be normalized so that the auto-correlations, i.e. the cross-correlation of a signal with itself, at zero lag are equal to 1. Cross-correlation coefficients range then from -1 to 1, ±1 being the maximum positive/negative correlation and 0 the minimum.

Normalized cross-correlation was calculated between the MUA firing rate and the power in several EEG frequency bands using the xcorr function in MATLAB with the parameter 'coeff' (see Figure 3). In order to do that, the firing rate was interpolated to match the time points of the EEG using the MATLAB function interp1. The studied EEG frequency bands were the following: Delta [1-4

Hz], Theta [4-8 Hz], Alpha [8-12 Hz], Beta [12-30 Hz], Low Gamma [30-50 Hz] and High Gamma [80-200 Hz]. To obtain the power in the bands, the EEG signal was band-pass filtered, squared, and subsequently low-pass filtered at 8 Hz – matching the 120 ms window for the MUA firing rate. MUA firing rate was correlated to the power in EEG channel 1 and channel 2, and to the added power of both channels.

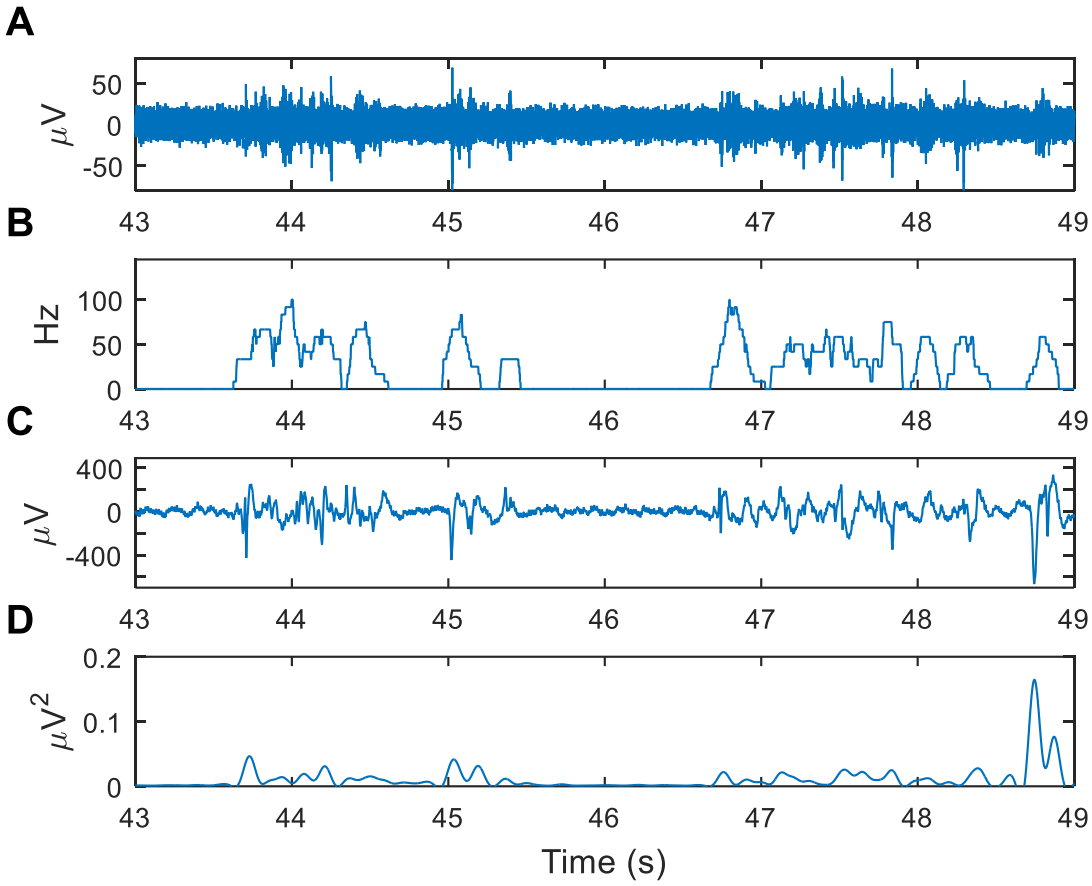

Figure 3. Sample segments of the correlated signals in 1.5% isoflurane. (A) MUA channel 1. (B) MUA firing rate. (C) EEG channel 1. (D) EEG channel 1 power.

2.4.4. Spike-Triggered Average

As defined by [31], "the spike-triggered average (STA) is a measure to relate a continuous signal and a simultaneously recorded spike train. It represents the average signal taken at the times of

spike occurrences …" Accordingly, 600 ms segments [32] centered around each spike were taken from the EEG and LFP signals, aligned, and averaged to obtain the corresponding STAs. Spikes detected earlier than 300 ms into the recording or later than 300 ms before the end of the recording were disregarded for this calculation.

To test for significance, 600 ms noise segments were taken and averaged. In this study, a noise segment was defined as a period of time in the EEG or LFP signals during which no action potentials were detected in the simultaneously recorded MUA, neither during the averaged 600 ms nor during the previous 200 ms and the posterior 60 ms.

2.4.5. Impulse Response

As discussed earlier, overlapping can be a difficult issue to overcome in detection and may affect measures such as the spike-triggered average. Impulse response (IR) is a measure reported to be unaffected by the temporal correlation of the spikes [33]. However, it is also very computationally expensive.

For this study, the IR, g, was calculated considering the spike train as a sequence of Dirac functions acting as the input, u, and the EEG/LFP acting as the output y (see Figure 4). Thus, at a given time point k:

$$y(k) = u(k-L)\cdot g(2L) + \cdots + u(k)\cdot g(L) + u(k+1)\cdot g(L-1) + \cdots + u(k+L-1)\cdot g(1)$$

where L is the number of samples to consider around each spike and $g(1) \ldots g(2L)$ are unknowns.

Solving for $n \geq 2L$ time samples we can form the following matrix equation:

$$\begin{bmatrix} u(k-L) & u(k-L+1) & \dots & u(k+L-1) \\ u(k-L+1) & u(k-L+2) & \dots & u(k+L) \\ \vdots & \vdots & \dots & \vdots \\ u(k-L+n-1) & u(k-L+n) & \dots & u(k+L+n-2) \end{bmatrix} \begin{bmatrix} g(2L) \\ g(2L-1) \\ \vdots \\ g(1) \end{bmatrix} = \begin{bmatrix} y(k) \\ y(k+1) \\ \vdots \\ y(k+n-1) \end{bmatrix}$$

With U and Y being the spike train and EEG/LFP matrices, respectively, we can isolate the impulse response matrix G as:

$$G = (U^T U)^{-1} U^T Y \tag{3}$$

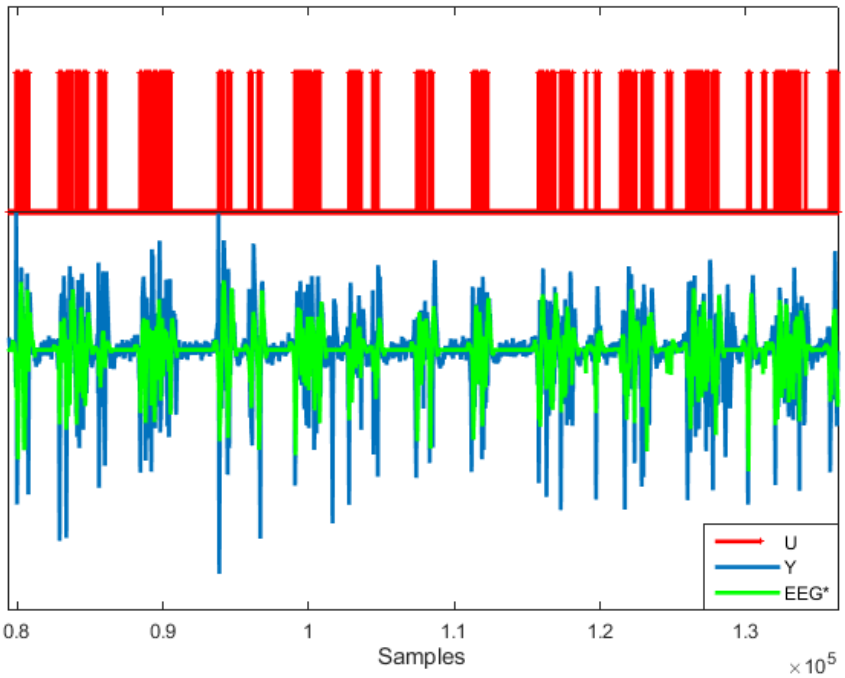

Figure 4. Impulse Response example on EEG. Spike train is treated as the input (U) and the EEG signal as the output (Y). EEG* is the predicted EEG, resulting from the convolution of the IR with the spike train.

To test for significance, the IR was also applied to the same noise segments used before for the STA.

2.4.6. Burst detection

In order to characterize the burst suppression pattern of the signals, bursts needed to be detected. What at first may seem a trivial task is, however, quite challenging. An algorithm was developed to automatically find bursts in both EEG and MUA signals. Manually detecting the bursts was also an option although it would have been extremely time-consuming, especially for the signals at low levels of anesthesia. Furthermore, it was important to ensure that the same criteria were followed throughout the whole dataset to be able to compare later on the occurrence and duration of bursts amongst anesthesia levels.

The algorithm detects a burst when the following conditions were met:

- The amplitude of the signal is greater than an input threshold, typically, 3 or 4 standard deviations greater than the mean of the signal.
- The signal goes back to baseline between bursts for at least a set amount of time. For EEG signals, the set time is 0.5 s [27] and for MUA signals 40 ms.

The output of the algorithm is the sample index of the beginning and end of the bursts, as shown in Figure 5.

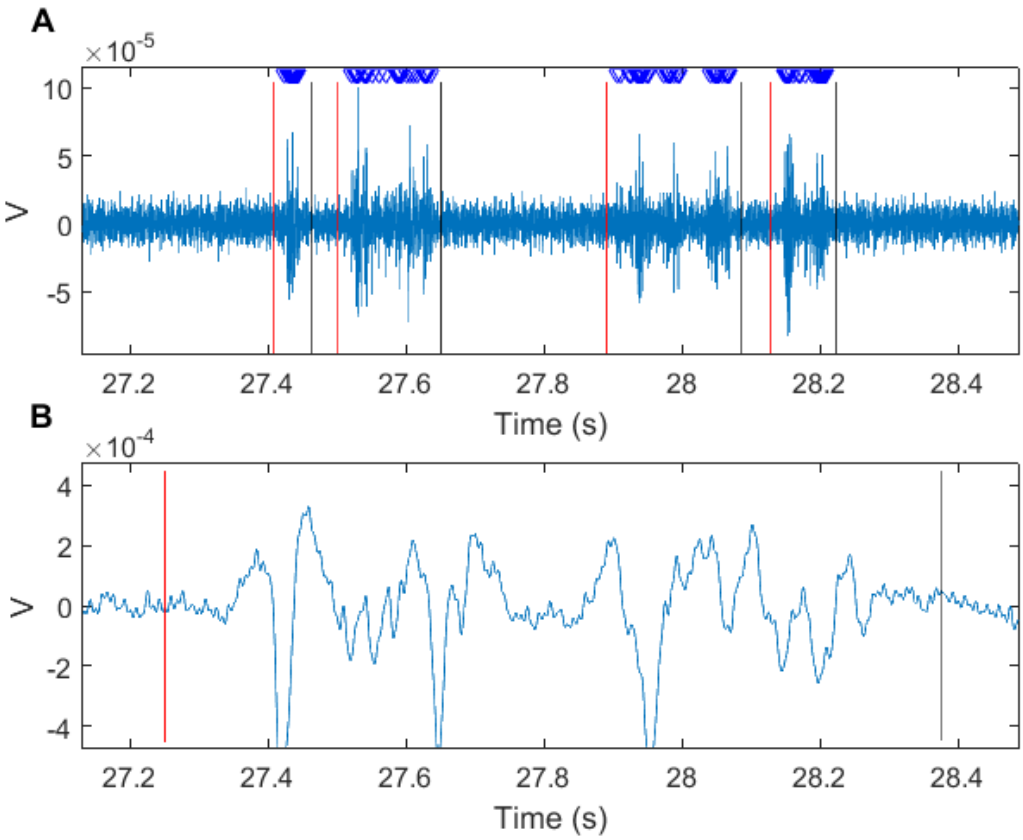

Figure 5. MUA and EEG burst detection example in the 2.5 % isoflurane signal. Red and black lines mark the beginning and the end of a burst, respectively. (A) MUA channel 1. Downward-pointing triangles represent the detected APs. (B) EEG channel 1.

CHAPTER 3

Results and Discussion

3.1. Characterization of the burst suppression pattern

The characterization of the EEG burst suppression pattern per isoflurane concentration percentage is summarized in the table below. Characterizing the burst suppression pattern is essential to determine the effects that isoflurane has on the signals across the different levels of anesthesia since, as mentioned earlier, the isoflurane concentration is not a good indicator of the depth of anesthesia at such high concentrations.

Table 2. EEG burst characterization per isoflurane concentration percentage: Burst suppression ratio (BSR) calculated in two-minute segments, isoflurane level based on BSR, burst occurrence in 10 s, burst duration and burst power. The first row, shadowed in gray, belongs to the baseline experiment, i.e., 4 min EEG recordings at each of the 8 heptode positions, while the rest of the data belongs to the isoflurane variation experiment. All data presented was taken from the same animal. (*) denotes no available statistics. N equals number of 10-second segments for the burst occurrence parameter and total number of bursts for the burst duration and burst power parameters.

Isoflurane %	BSR (mean ± SE)	Isoflurane level	Burst occurrence in 10 s (mean ± SE)	Burst duration (mean ± SE)	Burst power (mean ± SE)
1.5 %	46.80 ± 2.18 % (N = 16)	1	3.71 ± 0.16 (N = 194)	1.38 ± 0.06 s (N = 720)	58.33 ± 2.33 μV^2 (N = 720)
1.5 %	41.69 % (*)	1	4.00 ± 0.68 (N = 14)	1.39 ± 0.07 s (N = 56)	55.70 ± 8.04 μV^2 (N = 52)
1.5 %	50.47 % (*)	2	2.86 ± 0.90 (N = 7)	1.70 ± 0.26 s (N = 20)	70.78 ± 15.44 μV^2 (N = 20)
2.5 %	79.84 % (*)	3	2.33 ± 0.57 (N = 9)	0.82 ± 0.17 s (N = 21)	37.13 ± 8.24 μV^2 (N = 21)

The recordings at 3.5% isoflurane were discarded from further analysis because they had a burst suppression ratio of 100%. For the included concentrations, the burst suppression ratio was used to define the isoflurane level. Notice that, for the two 1.5% recordings in the isoflurane variation experiment, the burst suppression ratio is not within error of the 1.5% recording for the baseline experiment, one being less suppressed and the other one being more suppressed. That is the reason why three separate levels of anesthesia were established for the isoflurane variation experiment although the isoflurane concentration that the rat was inhaling was the same for levels 1 and 2. Firing frequency within the bursts was also affected by the increasing level of anesthesia (see Figure 6). The correlation coefficient between the firing frequency per EEG burst and the burst suppression ratio was 0.53 with a p-value of $5 \cdot 10^{-8}$. This suggests that, even though neurons fire less as the anesthesia deepens due to the longer suppression periods, they fire at a higher frequency.

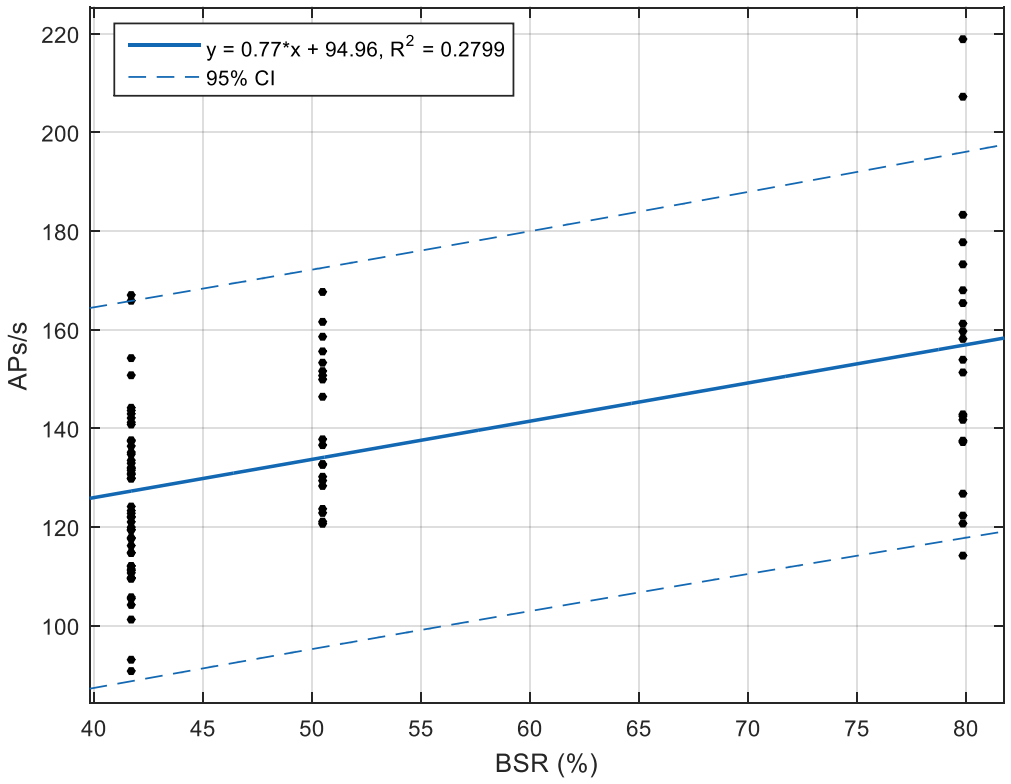

Figure 6. Frequency of action potentials per EEG burst vs. burst suppression ratio (BSR). Number of EEG bursts per BSR are 52, 20 and 21, respectively.

As for burst occurrence, burst duration, and burst power, the three 1.5% isoflurane recordings are within error of each other. However, all variables clearly decrease at the deepest level of anesthesia, which coincides with the findings reported in the literature [4], [27], [34], [35], [36].

3.2. Correlation between EEG and MUA

In this section, different analyses on the baseline experiment data are presented to show the coupling between the EEG and the MUA.

3.2.1. EEG as a spike predictor

A total of 45,121 action potentials were detected during approximately 32 minutes of recording under 1.5% isoflurane. Out of these 45,121, only 770 action potentials did not occur during an EEG burst, i.e. 1.7% of the spikes happened while the EEG was isoelectric. If we consider the EEG as a spike predictor, this translates into a true positive rate – the number of spikes during EEG bursts divided by the total number of spikes – of 98.3%. Furthermore, this rate may be undermined by the false positive errors of the spike detector and also relies on the burst detection accuracy. Despite these difficulties, based on the extremely high true positive rate, we can confidently conclude that EEG bursting in the setting of an anesthesia-induced burst suppression state implies the firing of neurons. Affirming the opposite, i.e. spiking implies that the EEG is bursting, is a little bit trickier even though it is true for most cases (98.3%). The action potentials that occur while the EEG is flat (see Figure 7) all have many traits in common such as spike amplitude across channels or dominant channel, even though they are averaged across all depth

microelectrode positions (see Figure 7C). This suggests that they all may have been fired by the same neuron or by neurons in the same network.

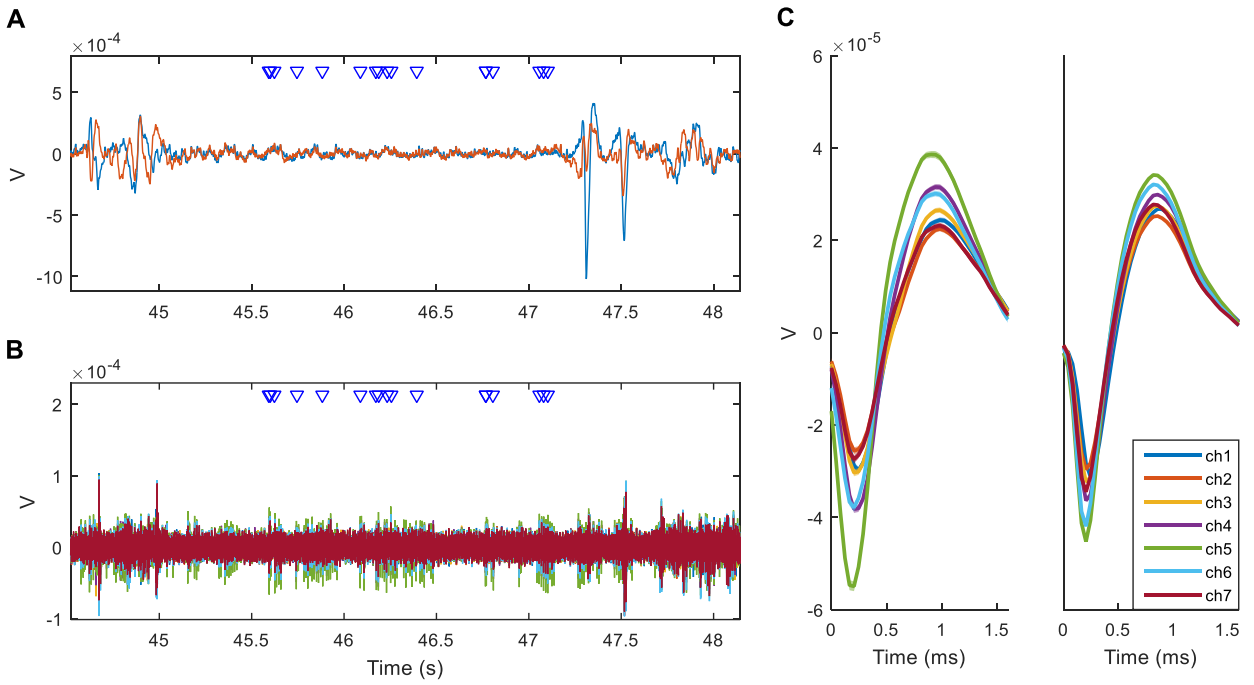

Figure 7. Presence of spikes during flat EEG. (A) EEG (channel 1 in blue and channel 2 in red). (B) MUA (7 channels). Downward-pointing triangles represent detected APs that occur during isoelectric EEG. (C) Average waveform of the 770 spikes under flat EEG (left) and the 44,351 spikes occurring during an EEG burst (right). Shading represents 95% confidence intervals.

3.2.2. Correlation across frequency bands

The results of the correlation analysis between EEG and MUA firing rates are shown in Figure 8. Averaging through all heptode positions is a valid procedure not only because the isoflurane concentration is the same, but also because the percentage of burst suppression is similar for all of them (recall Table 2) and no correlation trends related to the microelectrode depth were found.

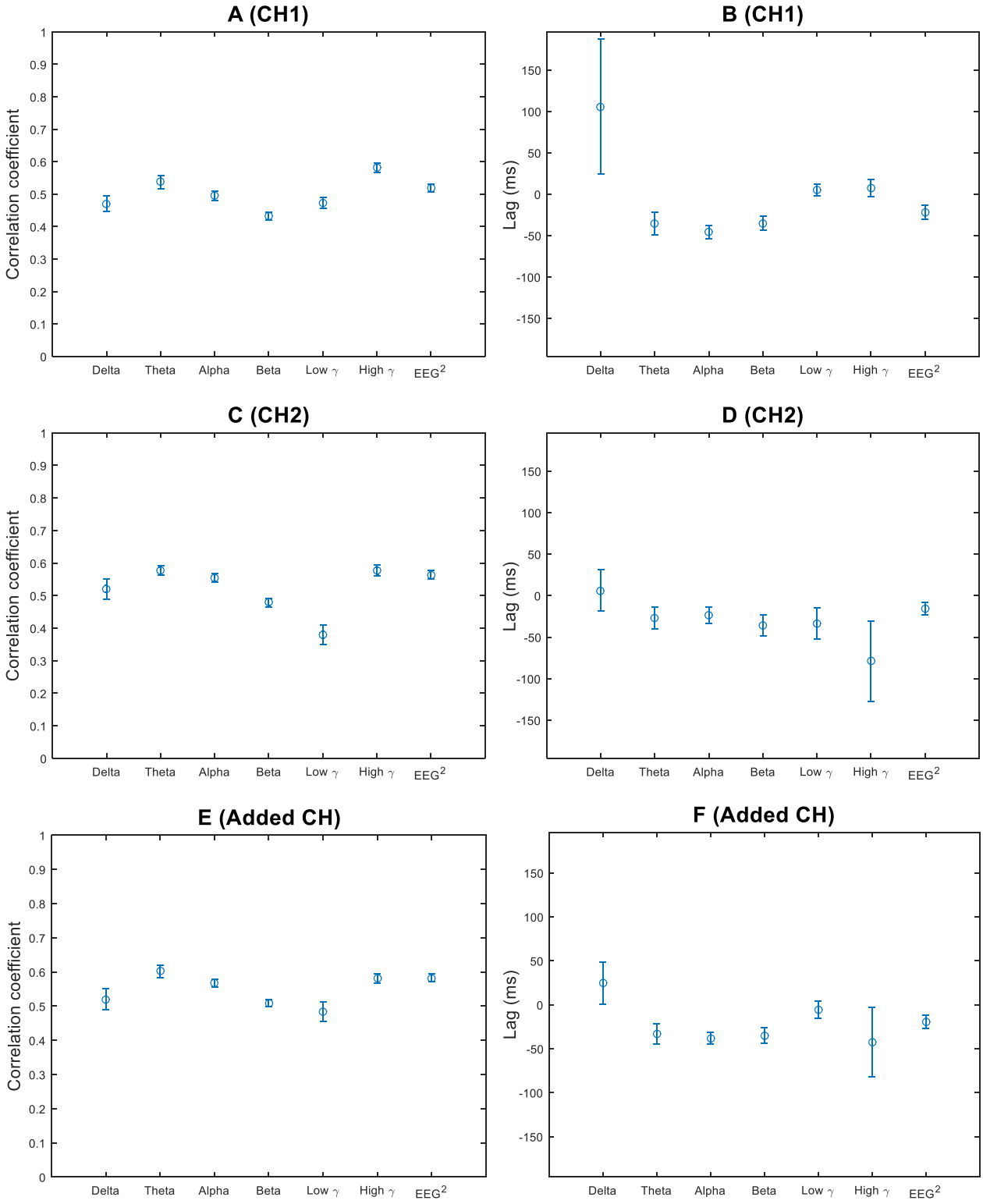

Figure 8. MUA firing rate vs. EEG cross-correlation for baseline experiment data averaged across heptode positions. (A) Maximum correlation coefficients for channel 1 of the EEG. (B) Lags at maximum correlation for EEG channel 1. (C) Maximum correlation coefficients for channel 2 of the EEG. (D) Lags at maximum correlation for EEG channel 2. (E) Maximum correlation coefficients for the two EEG channels added. (F) Lags at maximum correlation for the two EEG channels added. Negative lags indicate that the EEG follows the MUA firing rate. Error bars show 95% confidence intervals (N = 16: 2 two-minute recordings each at 8 heptode positions).

The action potential firing rates and EEG are highly correlated – with correlation coefficients above 0.3 in all the cases – even though the action potentials and EEG were recorded cross-hemisphere. High-gamma and theta power are the most correlated – with coefficients around 0.6 –, which matches previously reported findings that relate spiking activity to high-gamma power [37], and may also reflect the relationship between spiking and theta phase reported in [38].

Both EEG channels, separately and added, display the same trends. The fact that the added channels present higher correlation coefficients could imply that some of the neurons are more strongly correlated to one of the two channels. Lag in the high-gamma band is, however, not consistent across the two EEG channels. Whereas in general EEG precedes spiking in channel 1, spiking comes before EEG in channel 2. This could be explained by the position of the electrodes since channel 1 is closer to the site where spikes are being recorded.

3.2.3. STA and IR across positions

STA was computed on both the EEG and LFP signals to determine how coupled they are with the spikes considering that EEG was recorded in the opposite hemisphere from the spikes and the LFPs in the exact same location. IR was also applied to assure that the STA was a reliable measure and not being affected by overlapping spikes.

The LFP STA presents a very sharp drop approximately 100 ms before the spike (see Figure 9). This negative component is probably due to the decrease of sodium concentration in the extracellular space during the depolarization of the membrane of the neurons. The subsequent increase in voltage most likely reflects the hyperpolarization of the neurons [39].

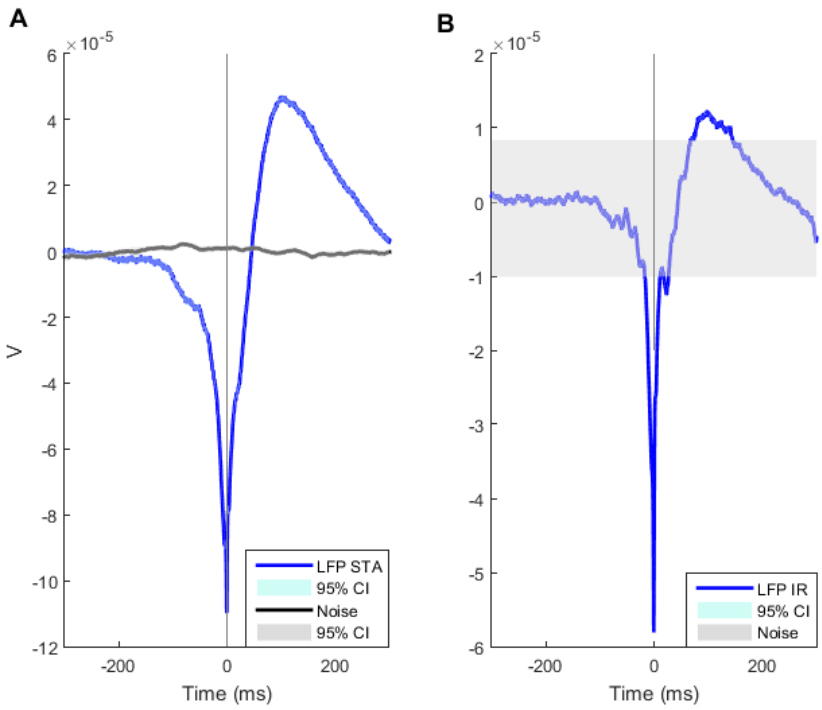

Figure 9. LFP STA and IR across all positions. Average of the 7 extracellular channels. Gray vertical lines represent the time of the AP peak. (A) STA, average of 44,908 spikes and 626 noise samples. (B) IR, average of 44,292 spikes. IR noise band shows maximum and minimum values of an average of 621 noise segments.

In [39], a small positive peak in the LFP STA prior to the negative deflection was also reported, possibly due to capacitive currents. Although this was not seen in the LFP STA (see Figure 9A), it did appear on the EEG channel 1 STA (see Figure 10A). Despite that, the LFP STA and EEG channel 1 STA have very similar waveforms and are consistent with other studies [29, Fig. 2A], [39, Fig. 5].

The higher response seen in the EEG STA for channel 1 relative to channel 2 (see Figure 10A, B) is reasonable, since the depth microelectrode recording the spikes is much closer to EEG channel 1. This could also explain the fact that for channel 1 the EEG response precedes the spike and for channel 2 follows the spike, which indeed matches the correlation results. However, in both cases, the STA shows a significant response, which is remarkable if we take into account that spikes and EEG are recorded cross-hemisphere. The higher response in the frontal channel

(channel 1) with respect to the occipital channel (channel 2) could also be accounting for the fact that, under anesthesia, alpha power is predominant in the frontal areas [3].

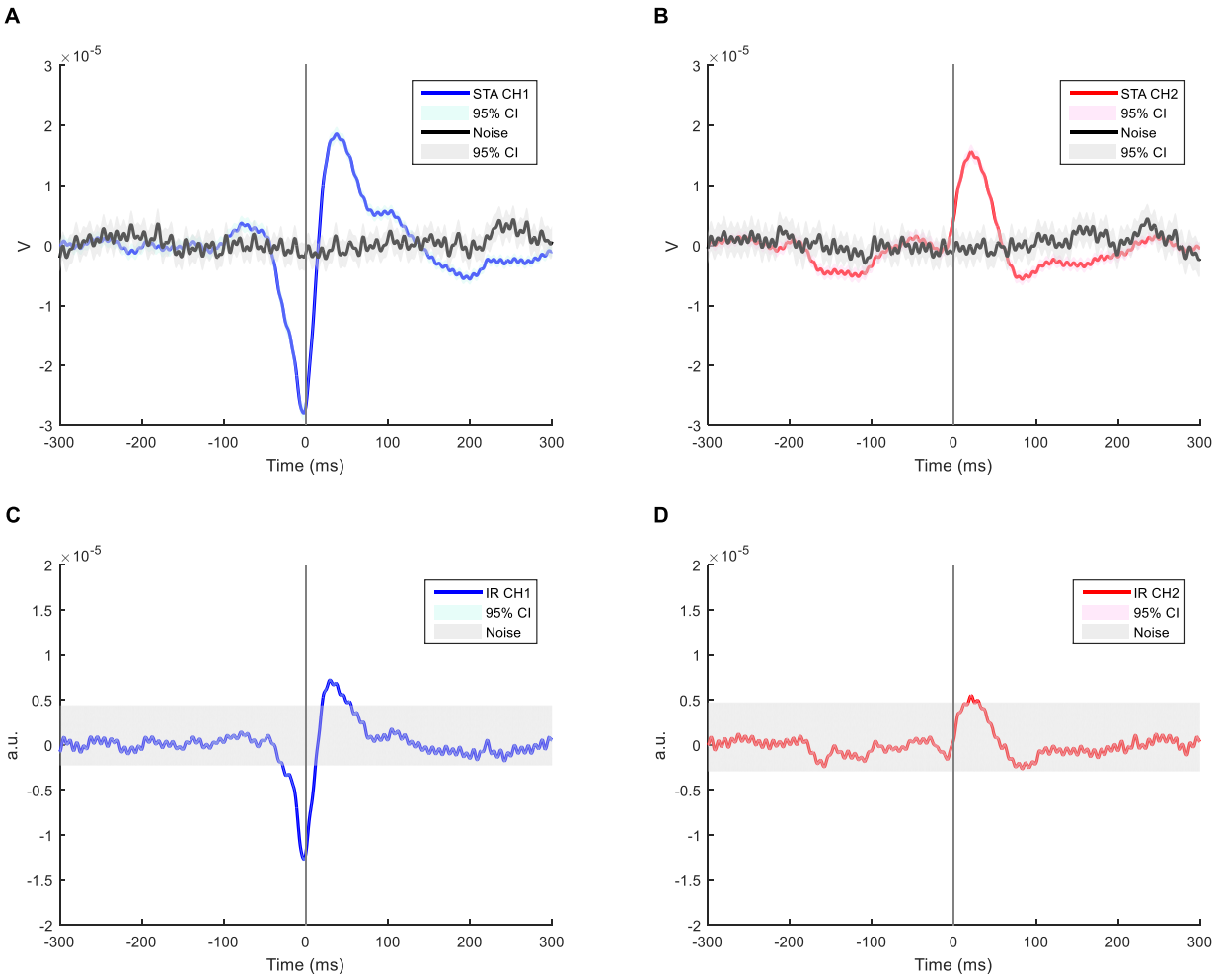

Figure 10. EEG STA and IR across all positions. Gray vertical lines show the time of the AP peak. (A) STA on channel 1 of the EEG. Average of 44,914 APs and 629 noise segments. (B) STA on channel 2 of the EEG. Average of 44,914 APs and 629 noise segments. (C) IR on channel 1 of the EEG. Average of 44,292 APs. (D) IR on channel 2 of the EEG. Average of 44,292 APs. IR noise bands show maximum and minimum values of an average of 618 noise segments.

The grand-average impulse response and spike-triggered average show the same response for both LFP and EEG (see Figure 9 and Figure 10). The fact that we obtain the same results with the two different techniques proves that the increase in amplitude around the spikes is not due to the occurrence of spikes insufficiently far apart. Proving significance using the IR technique is harder because arbitrary units make questionable averaging the different IR results across

heptode positions. Therefore, STA is the technique that will be used in the following analyses since spike overlapping does not influence the results.

Shown below (Figure 11-18) are the EEG STAs for sorted neurons across the eight positions of the depth microelectrode. As the position of the heptode changes, the same five neurons can be identified, with some additional neurons in the deeper positions (P3 – P8). The figures are color coded; manually matched neurons – based on the 7-channel average spike waveforms – are plotted in the same color.

Individually in a given position, not all neurons show the same STA response (see green neuron in position 2 – Figure 12 – for a clear example), which has been previously related to different functional roles in a network [32]. Notice that, across all positions, the blue, red, and purple neurons consistently have similar STAs and the highest numbers of action potentials fired, contributing the most to the grand-average EEG STA.

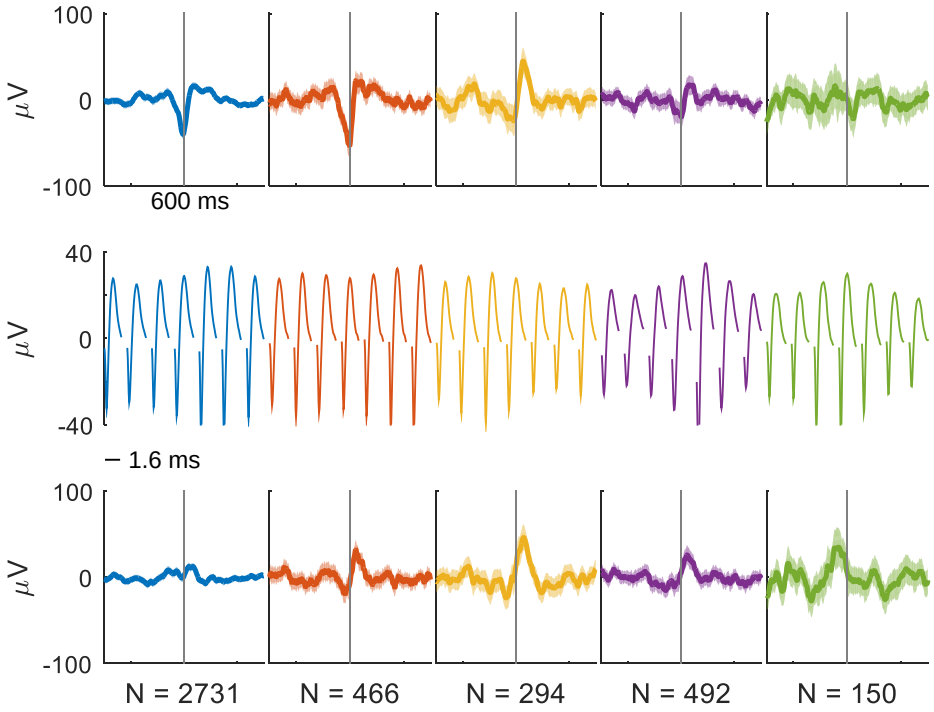

Figure 11. P1 (1710 μm) sorted STA and spikes. EEG channel 1 (top) and channel 2 (bottom) STA for 5 individual neurons. (Middle) Average spike waveform for each neuron and each of the 7 channels. N is the number of detected spikes for each neuron, which was used to obtain the STAs and average waveforms. Shaded area around the STAs shows the 95% CI. Gray vertical lines show the time of the AP peak.

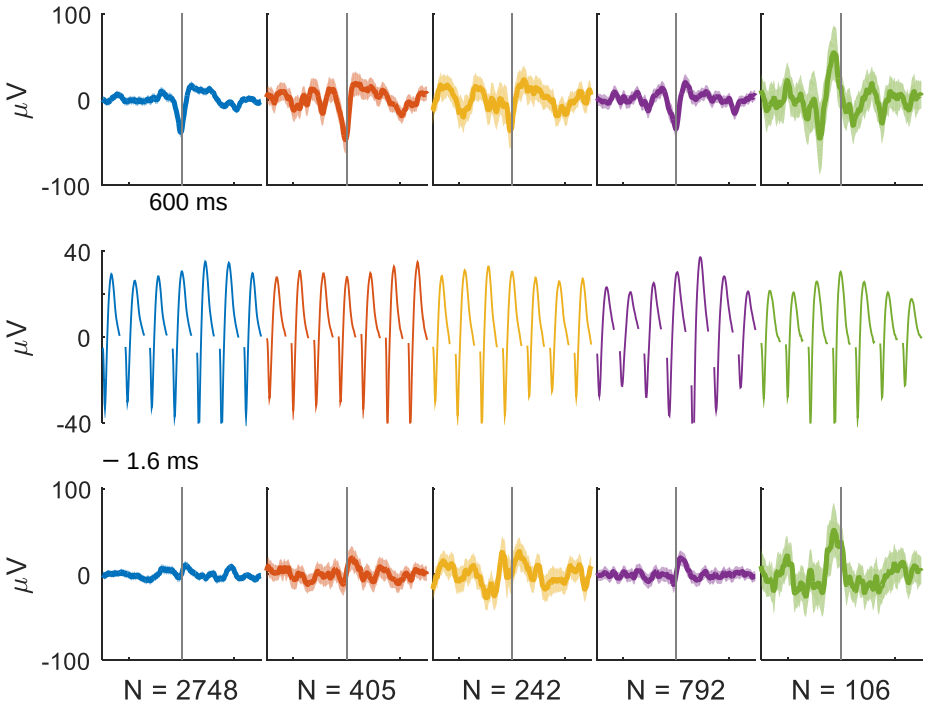

Figure 12. P2 (1720 μm) sorted STA and spikes. EEG channel 1 (top) and channel 2 (bottom) STA for 5 individual neurons. (Middle) Average spike waveform for each neuron and each of the 7 channels. N is the number of detected spikes for each neuron, which was used to obtain the STAs and average waveforms. Shaded area around the STAs shows the 95% CI. Gray vertical lines show the time of the AP peak.

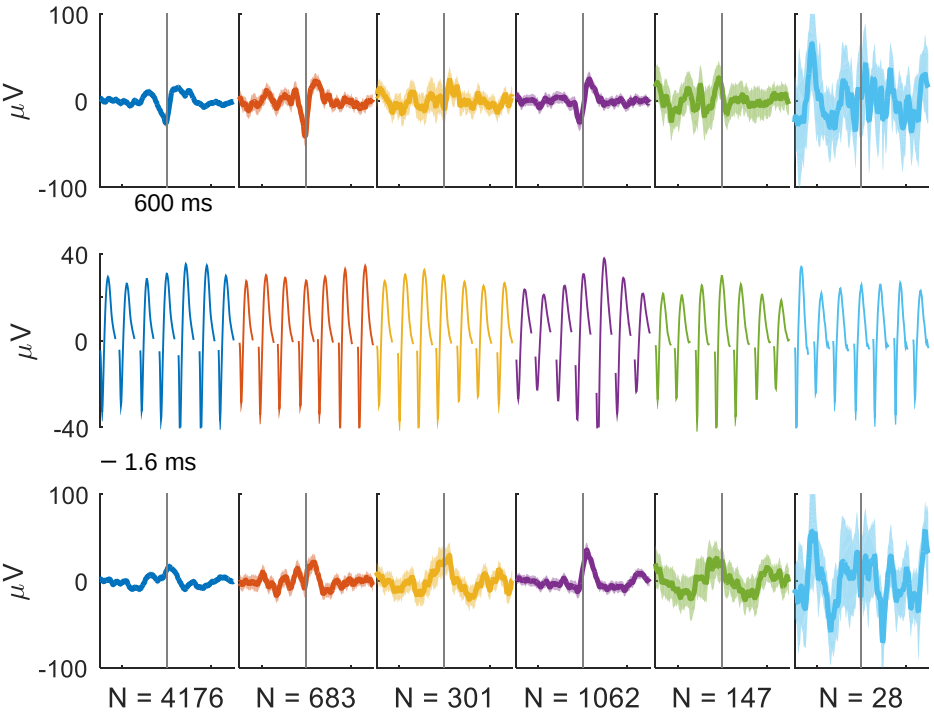

Figure 13. P3 (1730 μm) sorted STA and spikes. EEG channel 1 (top) and channel 2 (bottom) STA for 6 individual neurons. (Middle) Average spike waveform for each neuron and each of the 7 channels. N is the number of detected spikes for each neuron, which was used to obtain the STAs and average waveforms. Shaded area around the STAs shows the 95% CI. Gray vertical lines show the time of the AP peak.

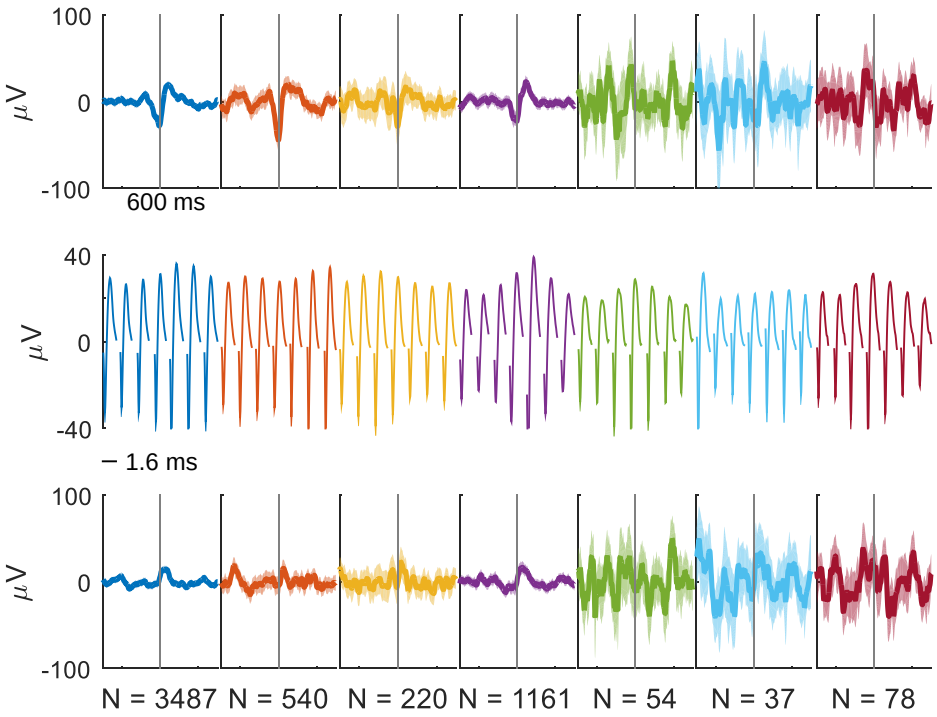

Figure 14. P4 (1740 μm) sorted STA and spikes. EEG channel 1 (top) and channel 2 (bottom) STA for 7 individual neurons. (Middle) Average spike waveform for each neuron and each of the 7 channels. N is the number of detected spikes for each neuron, which was used to obtain the STAs and average waveforms. Shaded area around the STAs shows the 95% CI. Gray vertical lines show the time of the AP peak.

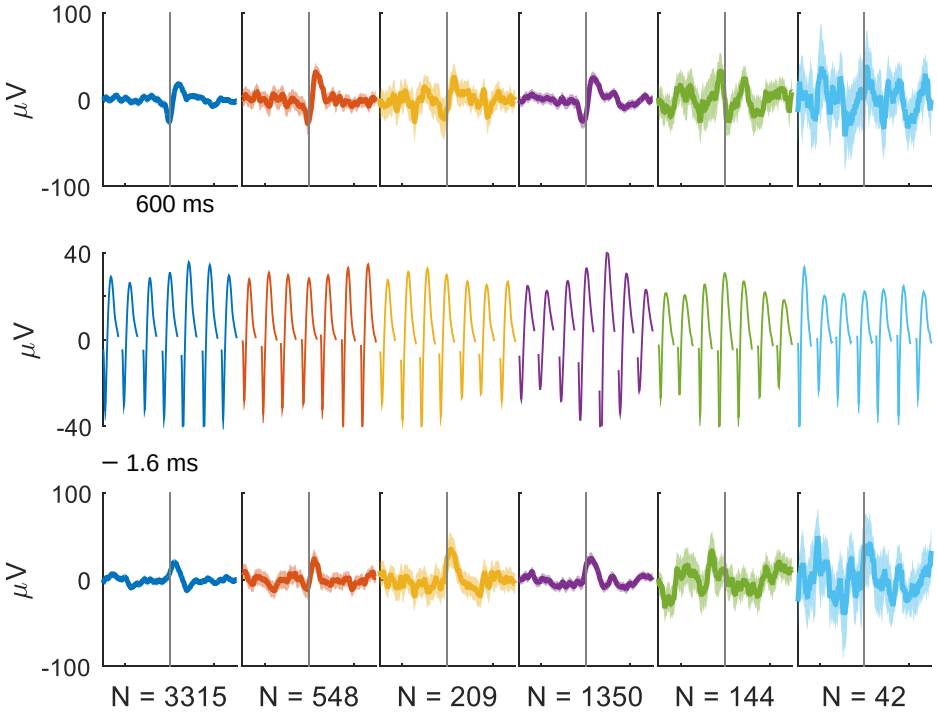

Figure 15. P5 (1750 μm) sorted STA and spikes. EEG channel 1 (top) and channel 2 (bottom) STA for 6 individual neurons. (Middle) Average spike waveform for each neuron and each of the 7 channels. N is the number of detected spikes for each neuron, which was used to obtain the STAs and average waveforms. Shaded area around the STAs shows the 95% CI. Gray vertical lines show the time of the AP peak.

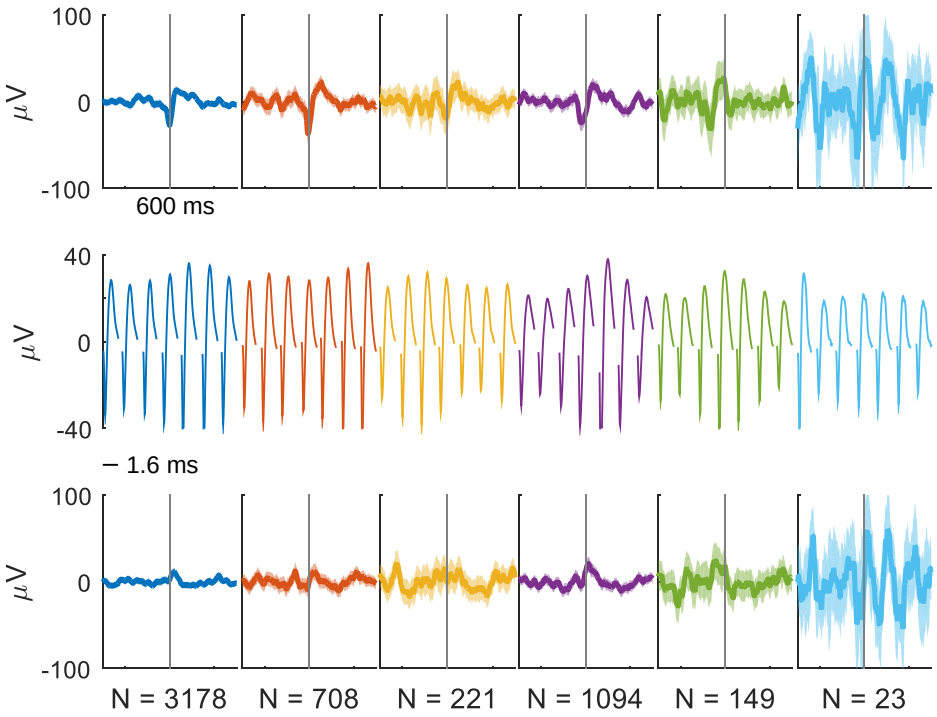

Figure 16. P6 (1760 μm) sorted STA and spikes. EEG channel 1 (top) and channel 2 (bottom) STA for 6 individual neurons. (Middle) Average spike waveform for each neuron and each of the 7 channels. N is the number of detected spikes for each neuron, which was used to obtain the STAs and average waveforms. Shaded area around the STAs shows the 95% CI. Gray vertical lines show the time of the AP peak.

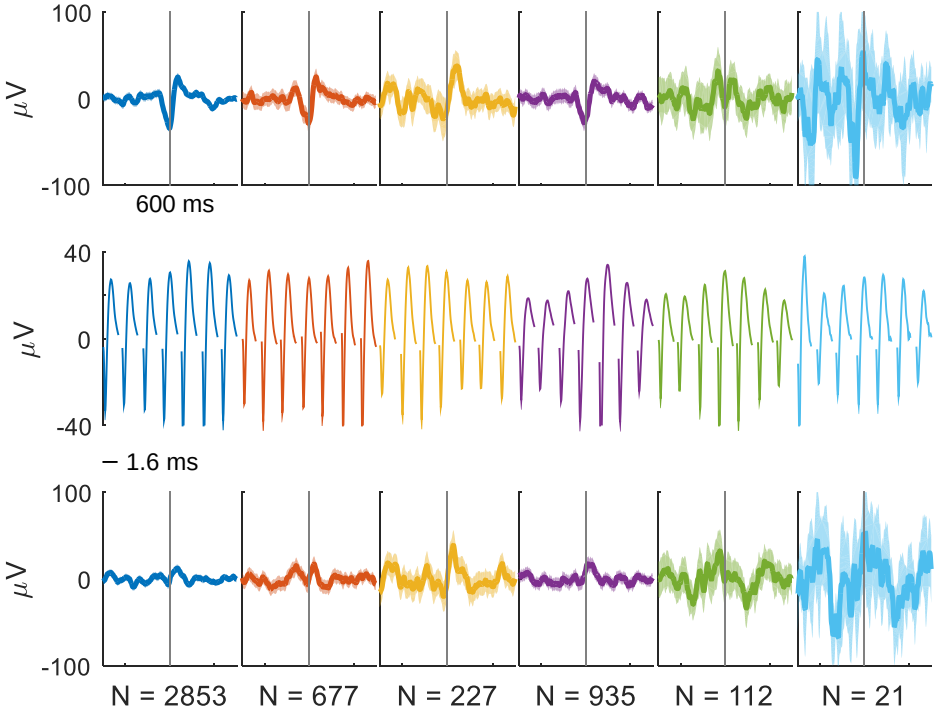

Figure 17. P7 (1770 μm) sorted STA and spikes. EEG channel 1 (top) and channel 2 (bottom) STA for 6 individual neurons. (Middle) Average spike waveform for each neuron and each of the 7 channels. N is the number of detected spikes for each neuron, which was used to obtain the STAs and average waveforms. Shaded area around the STAs shows the 95% CI. Gray vertical lines show the time of the AP peak.

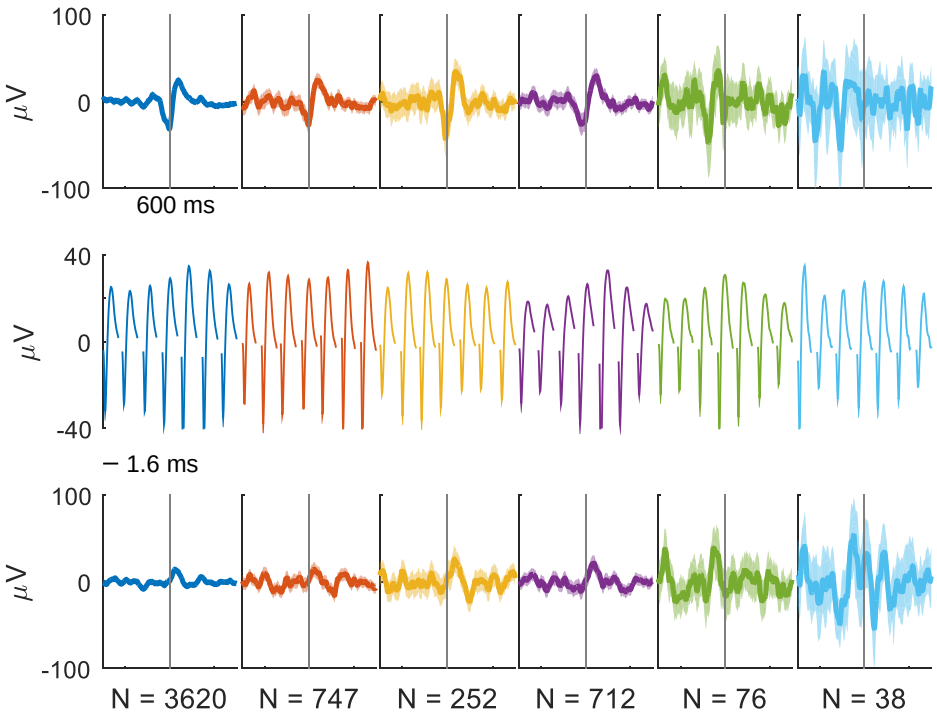

Figure 18. P8 (1780 μm) sorted STA and spikes. EEG channel 1 (top) and channel 2 (bottom) STA for 6 individual neurons. (Middle) Average spike waveform for each neuron and each of the 7 channels. N is the number of detected spikes for each neuron, which was used to obtain the STAs and average waveforms. Shaded area around the STAs shows the 95% CI. Gray vertical lines show the time of the AP peak.

3.3. Effect of the anesthesia concentration

In this section, different analyses of the data from the isoflurane variation experiment are presented to show the effects that increasing levels of anesthesia have on the EEG, the LFP, the MUA, and their relationship.

The LFP STA shows an increase in amplitude as the anesthesia deepens (see Figure 19), which has also been reported in [40]. However, we are not seeing this increase only on the LFP STA but also in the EEG STA (see Figure 20). This finding may imply that the connectivity across hemispheres is enhanced since EEG is recorded in the left hemisphere while spikes are recorded in the right hemisphere. This increase in connectivity may be due to neurons becoming more phase-locked and therefore showing a stronger response when averaging around the spikes. The

spike-like waveform that averaging brings out in the LFP deflection at the time of the spike has been reported as a common residual from the spikes into the LFP signals due to the insufficiency of low pass filtering to separate the LFPs from the spikes [41], [42].

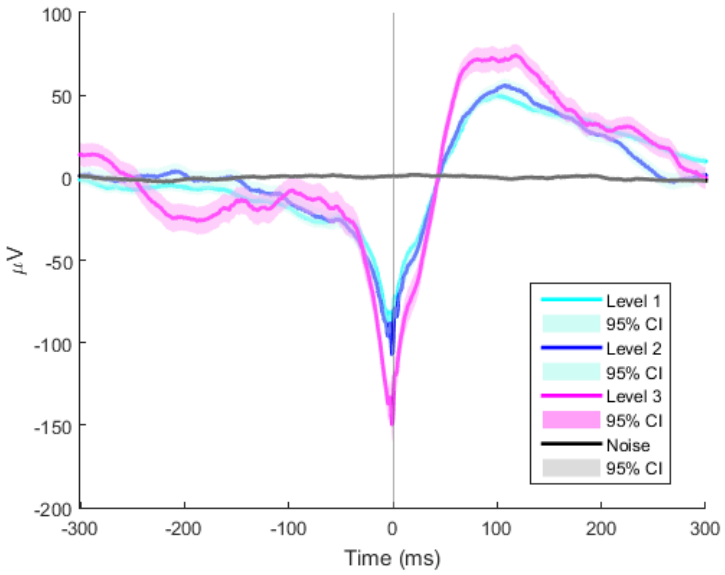

Figure 19. LFP STA for varying levels of anesthesia. The gray vertical line shows the time of the AP peak. LFP STA for isoflurane levels 1, 2 and 3, averaged over 5,645, 2,624 and 1,107 APs, respectively, and 294 noise segments.

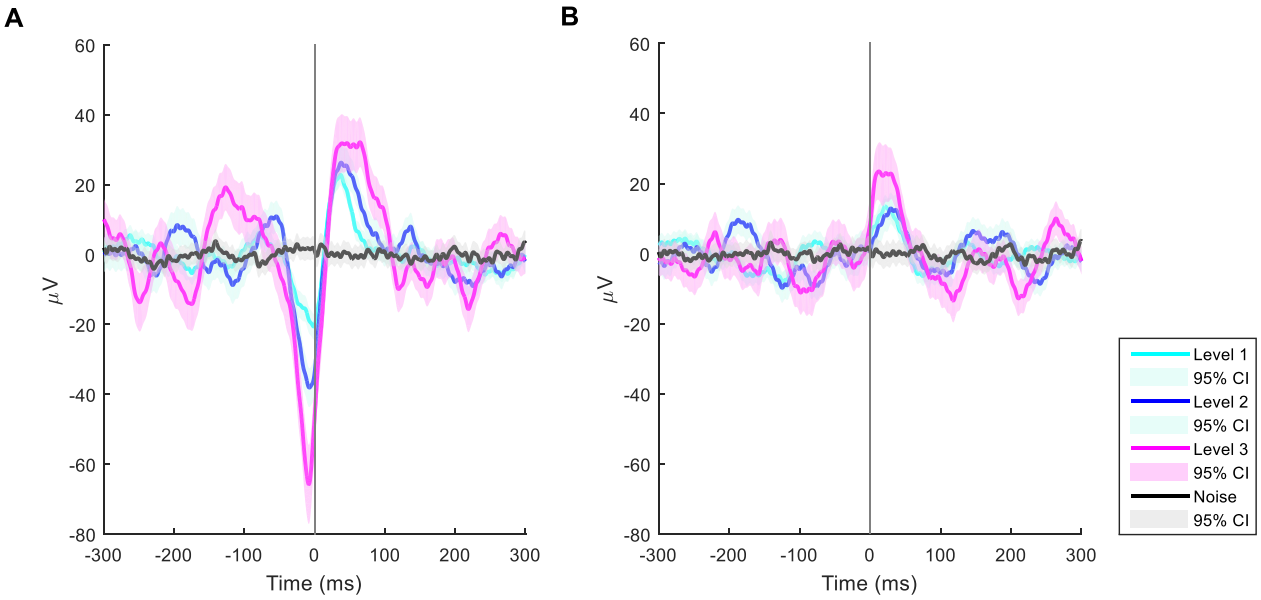

Figure 20. EEG STA for varying levels of anesthesia. The gray vertical lines show the time of the AP peak. STA of the EEG for isoflurane levels 1, 2 and 3, averaged over 5,645, 2,624 and 1,107 APs, respectively, and 295 noise segments from all three levels. (A) STA on channel 1 of the EEG. (B) STA on channel 2 of the EEG.

The fact that we see the same increase in STA amplitude as the anesthesia deepens as [40] is meaningful because we are using another type of anesthetic – isoflurane instead of propofol –, and it is not only shown on the LFP but also on the EEG – which is recorded in the opposite hemisphere. Moreover, the effect can be seen on individual neurons matched across anesthesia levels (see Figure 21-23). Like before, manually matched neurons are color-coded. EEG STA amplitudes clearly increase with the concentration of anesthesia administered.

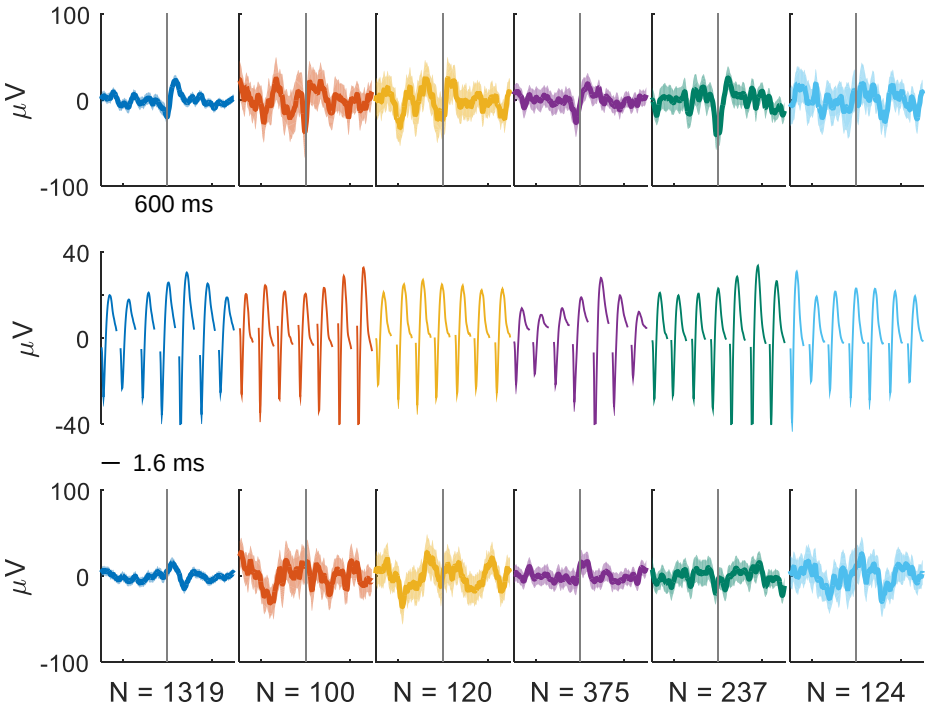

Figure 21. Isoflurane level 1 (1.5%) sorted STA and spikes. EEG channel 1 (top) and channel 2 (bottom) STA for 6 individual neurons. (Middle) Average spike waveform for each neuron and each of the 7 channels. N is the number of detected spikes for each neuron, which was used to obtain the STAs and average waveforms. Shaded area around the STAs shows the 95% CI. Gray vertical lines show the time of the AP peak.

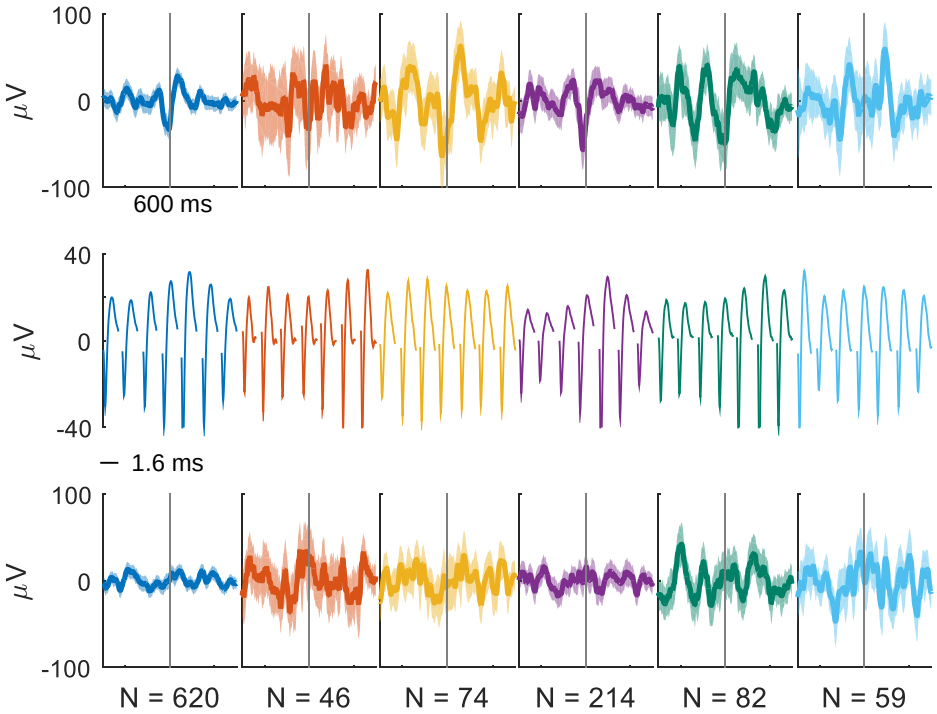

Figure 22. Isoflurane level 2 (1.5%) sorted STA and spikes. EEG channel 1 (top) and channel 2 (bottom) STA for 6 individual neurons. (Middle) Average spike waveform for each neuron and each of the 7 channels. N is the number of detected spikes for each neuron, which was used to obtain the STAs and average waveforms. Shaded area around the STAs shows the 95% CI. Gray vertical lines show the time of the AP peak.

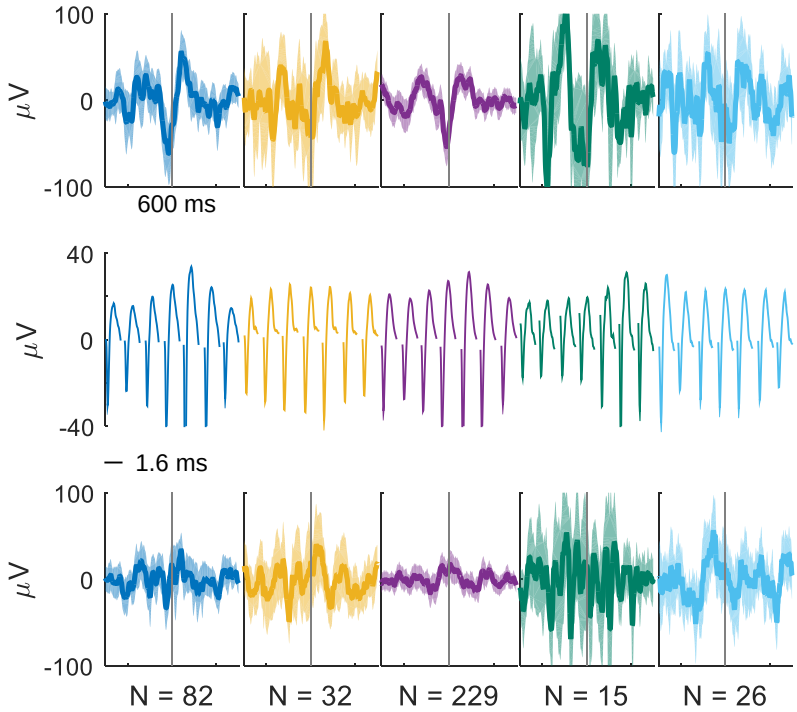

Figure 23. Isoflurane level 3 (2.5%) sorted STA and spikes. EEG channel 1 (top) and channel 2 (bottom) STA for 5 individual neurons. (Middle) Average spike waveform for each neuron and each of the 7 channels. N is the number of detected spikes for each neuron, which was used to obtain the STAs and average waveforms. Shaded area around the STAs shows the 95% CI. Gray vertical lines show the time of the AP peak.

Notice that 5 out of the 6 sorted neurons for 1.5% isoflurane are also firing at 2.5%, which suggests that anesthesia does not silence part of the neuronal population but instead causes less firing. A reason why the red neuron may be missing in 2.5% isoflurane is that there might not be enough waveforms characteristic to this neuron for the sorting algorithm to classify it since we can see that it is the neuron that fires the least at 1.5% isoflurane.

Individual neurons firing less is one of the known effects of anesthetics [43], however we have also seen that overall when they do, they fire at a higher firing rate (recall Figure 6).

CHAPTER 4

Conclusion and Future Work

EEG signals and MUA are closely related, as shown by the high correlation coefficients between the two and the spike prediction rate. This relationship seems to be further enhanced by anesthesia. EEG and LFP spike-triggered averages increase in amplitude with anesthesia, implying an increase in global connectivity as anesthesia deepens.

Also, as the isoflurane level increases, there are more isoelectric EEG segments – the burst suppression ratio increases – and, therefore, the number of spikes decreases, but the firing frequency in the bursts increases.

The decrease in cortical activity due to anesthesia is caused by a generalized decrease in firing of the neurons due to the suppression periods, as opposed to fewer neurons firing.

This thesis presents data from one animal only so, even though the results are promising, this type of study requires a larger sample of specimens to make any general claims. Acquiring data from more animals would be the first step towards continuing the work started here. This thesis has been a learning process in many aspects from experimental procedures to analysis techniques. We now have a better understanding of how powerful and revealing is the simultaneous recording of brain signals at two different scales and that is why it is worth continuing

the analysis. One possible direction would be to examine the sub-delta range of the signals or ultra-slow waves, i.e. from 0.1 to 1 Hz, which is thought to be relevant in several grades of coma. It would also be interesting to study the long range connectivity under isoflurane by placing the electrodes further apart from each other to study the interaction between distant regions of the brain – e.g. frontal and occipital – since it is known that anesthesia effects do not happen uniformly across the cortex.

BIBLIOGRAPHY

[1] D. H. Robinson and A. H. Toledo, “Historical Development of Modern Anesthesia,” *J. Investig. Surg.*, vol. 25, no. 3, pp. 141–149, 2012.

[2] M. T. Alkire, A. G. Hudetz, and G. Tononi, “Consciousness and Anesthesia,” *Science*, vol. 322, no. 5903, pp. 876–880, 2008.

[3] P. L. Purdon, E. T. Pierce, E. A. Mukamel, M. J. Prerau, J. L. Walsh, K. Wong, A. F. Salazar-Gomez, P. G. Harrell, A. L. Sampson, A. Cimenser, S. Ching, N. J. Kopell, C. Tavares-Stoeckel, K. Habeeb, R. Merhar, and E. N. Brown, “Electroencephalogram signatures of loss and recovery of consciousness from propofol,” *Proc. Natl. Acad. Sci.*, vol. 110, no. 12, pp. E1142–E1151, 2013.

[4] J. Bruhn, H. Röpcke, B. Rehberg, T. Bouillon, and A. Hoeft, “Electroencephalogram Approximate Entropy Correctly Classifies the Occurrence of Burst Suppression Pattern as Increasing Anesthetic Drug Effect,” *Anesthesiology*, vol. 93, no. 4, pp. 981–985, 2000.

[5] M. Milh, H. Becq, N. Villeneuve, Y. Ben-Ari, and L. Aniksztejn, “Inhibition of Glutamate Transporters Results in a ‘ Suppression-Burst ’ Pattern and Partial Seizures in the Newborn Rat,” *Epilepsia*, vol. 48, no. 1, pp. 169–174, 2007.

[6] J. Rakesh, J. A. Sgro, A. R. Towne, D. Ko, and R. J. DeLorenzo, “Prognostic Value of EEG Monitoring After Status Epilepticus: A Prospective Adult Study,” *J. Clin. Neurophysiol.*, vol. 14, no. 4, pp. 326–334, 1997.

[7] Y. Kuroiwa and G. G. Celesia, “Clinical Significance of Periodic EEG Patterns,” *Arch. Neurol.*, vol. 37, no. 1, pp. 15–20, 1980.

[8] E. C. Leuthardt, G. Schalk, J. R. Wolpaw, J. G. Ojemann, and D. W. Moran, “A brain-computer interface using electrocorticographic signals in humans,” *J. Neural Eng.*, vol. 1, no. 2, pp. 63–71, 2004.

[9] G. Schalk and J. Mellinger, “Brain Sensors and Signals,” in *A Practical Guide to Brain-Computer Interfacing with BCI2000*, Springer-Verlag London Limited 2010, 2010, pp. 9–35.

[10] C. Bédard, K. Helmut, and A. Destexhe, “Modeling Extracellular Field Potentials and the Frequency-Filtering Properties of Extracellular Space,” *Biophys. J.*, vol. 86, pp. 1829–1842, 2004.

[11] S. Katzner, I. Nauhaus, A. Benucci, V. Bonin, D. L. Ringach, and M. Carandini, “Local Origin of Field Potentials in Visual Cortex,” *Neuron*, vol. 61, no. 1, pp. 35–41, 2009.

[12] D. Xing, C.-I. Yeh, and R. M. Shapley, “Spatial Spread of the Local Field Potential and its Laminar Variation in Visual Cortex,” *J. Neurosci.*, vol. 29, no. 37, pp. 11540–11549, 2009.

[13] Y. Kajikawa and C. E. Schroeder, “How local is the local field potential?,” *Neuron*, vol. 72, no. 5, pp. 847–858, 2011.

[14] I. Nauhaus, L. Busse, C. M, and D. Ringach, “Stimulus contrast modulates functional connectivity in visual cortex,” *Nat. Neurosci.*, vol. 12, no. 1, pp. 70–76, 2009.

[15] G. Buzsáki, C. A. Anastassiou, and C. Koch, “The origin of extracellular fields and currents — EEG , ECoG , LFP and spikes,” *Nat. Rev. Neurosci.*, vol. 13, pp. 407–420, 2012.

[16] C. Gold, D. A. Henze, C. Koch, and G. Buzsáki, “On the Origin of the Extracellular Action Potential Waveform : A Modeling Study On the Origin of the Extracellular Action Potential Waveform : A Modeling Study,” *J. Neurophysiol.*, vol. 95, no. 5, pp. 3113–3128, 2006.

[17] L. Voss and J. Sleigh, “Monitoring consciousness: the current status of EEG-based depth of anesthesia monitors.,” *Best Pract. Res. Clin. Anesthesiol.*, vol. 21, no. 3, pp. 313–325, 2007.

[18] C. R. Ries and E. Puil, “Mechanism of Anesthesia Revealed by Shunting Actions of Isoflurane on Thalamocortical Neurons,” *J. Neurophysiol.*, vol. 81, no. 4, pp. 1795–1801, Apr. 1999.

[19] E. N. Brown, R. Lydic, and N. D. Schiff, “General Anesthesia, Sleep, and Coma,” *N Engl J Med*, vol. 363, no. 27, pp. 2638–2650, 2010.

[20] F. Jia, M. Yue, D. Chandra, G. E. Homanics, P. A. Goldstein, and N. L. Harrison, “Isoflurane Is a Potent Modulator of Extrasynaptic GABAA Receptors in the Thalamus,” *J. Pharmacol. Exp. Ther.*, vol. 324, no. 3, pp. 1127–1135, 2008.

[21] T. Bouillon and S. L. Shafer, “Does Size Matter?,” *Anesthesiology*, vol. 89, pp. 557–560, 1998.

[22] M. Osawa, K. Shingu, M. Murakawa, T. Adachi, J. Kurata, N. Seo, T. Murayama, S. Nakao, and K. Mori, “Effects of Sevoflurane on Central Nervous System Electrical Activity in Cats,” *Anesth. Analg.*, vol. 79, pp. 52–57, 1994.

[23] G. Paxinos and C. Watson, *The rat brain in stereotaxic coordinates*, 5th editio. Elsevier, Academic Press, 2004.

[24] H. Y. Seong, J. Y. Cho, B. S. Choi, J. K. Min, Y. H. Kim, S. W. Roh, J. H. Kim, and S. R. Jeon, “Analysis on Bilateral Hindlimb Mapping in Motor Cortex of the Rat by an Intracortical Microstimulation Method,” *J. Korean Med. Sci.*, vol. 29, no. 4, pp. 587–592, 2014.

[25] C. M. Gray, P. E. Maldonado, M. Wilson, and B. McNaughton, “Tetrodes markedly improve the reliability and yield of multiple single-unit isolation from multi-unit recordings in cat striate cortex,” *J. Neurosci. Methods*, vol. 63, no. 1–2, pp. 43–54, 1995.

[26] I. J. Rampil, R. B. Welskopf, J. G. Brown, E. I. Eger, B. H. Johnson, M. A. Holmes, and J. H. Donegan, “I653 and Isoflurane Produce Similar Dose-related Changes in the Electroencephalogram of Pigs,” *Anesthesiology*, vol. 69, no. 3, pp. 298–302, 1988.

[27] P. W. Doyle and B. F. Matta, “Burst suppression or isoelectric encephalogram for cerebral protection : evidence from metabolic suppression studies,” *Br. J. Anesth.*, vol. 83, no. 4, pp. 580–584, 1999.

[28] A. F. Szymanska, M. Doty, K. V Scannell, and Z. Nenadic, “A Supervised Multi-Sensor Matched Filter for the Detection of Extracellular Action Potentials,” in *2014 36th Annual International Conference of the IEEE Engineering in Medicine and Biology Society*, 2014, pp. 5996–5999.

[29] M. S. Lewicki, “A review of methods for spike sorting : the detection and classification of neural action potentials,” *Comput. Neural Syst.*, vol. 9, pp. R53–R78, 1998.

[30] A. A. Szymanska, A. Hajirasooliha, and Z. Nenadic, “Source Location as a Feature for the Classification of Multi-sensor Extracellular Action Potentials,” in *6th Annual International IEEE EMBS Conference on Neural Engineering*, 2013, pp. 235–238.

[31] J. Ito, “Spike-Triggered Average,” in *Encyclopedia of Computational Neuroscience*, D. Jaeger and R. Jung, Eds. New York, NY: Springer New York, 2013, pp. 1–5.

[32] A. C. Snyder and M. a. Smith, “Stimulus-dependent spiking relationships with the EEG,” *J. Neurophysiol.*, vol. 114, no. 3, pp. 1468–1482, 2015.

[33] B. A. Lopour, R. J. Staba, J. M. Stern, I. Fried, and D. L. Ringach, “Characterization of long-range functional connectivity in epileptic networks by neuronal spike-triggered local field potentials,” *J. Neural Eng.*, vol. 13, p. 026031, 2016.

[34] A. Romanov, R. Moon, M. Wang, and S. Joshi, “Paradoxical Increase in the Bispectral Index during Deep Anesthesia in New Zealand White Rabbits,” *J. Am. Assoc. Lab. Anim. Sci.*, vol. 53, no. 1, pp. 74–80, 2014.

[35] W. P. Akrawi, J. C. Drummond, C. J. Kalkman, and P. M. Patel, “A Comparison of the Electrophysiologic Characteristics of EEG Burst-Suppression as Produced by Isoflurane, Thiopental, Etomidate, and Propofol,” *J. Neurosurg. Anesthesiol.*, vol. 8, no. 1, pp. 40–46, 1996.

[36] K. M. Hartikainen, M. Rorarius, J. J. Peräkylä, P. J. Laippala, and V. Jäntti, “Cortical Reactivity During Isoflurane Burst-Suppression Anesthesia,” *Anesth. Analg.*, vol. 81, no. 6, pp. 1223–1228, 1995.

[37] S. Ray and J. H. R. Maunsell, “Different Origins of Gamma Rhythm and High-Gamma Activity in Macaque Visual Cortex,” *PLoS Biol.*, vol. 9, no. 4, p. e1000610, 2011.

[38] S. E. Fox, S. Wolfson, and J. B. Ranck, “Hippocampal theta rhythm and the firing of neurons in walking and urethane anesthetized rats,” *Exp. Brain Res.*, vol. 62, no. 3, pp. 495–508, 1986.

[39] S. Ray, S. S. Hsiao, N. E. Crone, P. J. Franaszczuk, and E. Niebur, “Effect of Stimulus Intensity on the Spike – Local Field Potential Relationship in the Secondary Somatosensory Cortex,” *J. Neurosci.*, vol. 28, no. 29, pp. 7334–7343, 2008.

[40] S. J. Hanrahan, B. Greger, R. A. Parker, T. Ogura, S. Obara, T. D. Egan, and P. A. House, “The effects of propofol on local field potential spectra , action potential firing rate , and their temporal relationship in humans and felines,” *Front. Hum. Neurosci.*, vol. 7, 2013.

[41] T. P. Zanos, P. J. Mineault, C. C. Pack, T. P. Zanos, P. J. Mineault, and C. C. Pack, “Removal of Spurious Correlations Between Spikes and Local Field Potentials,” *J. Neurophysiol.*, vol. 105, pp. 474–486, 2011.

[42] G. T. Einevoll, C. Kayser, N. K. Logothetis, and S. Panzeri, “Modelling and analysis of local field potentials for studying the function of cortical circuits,” *Nat. Rev. Neurosci.*, vol. 14, pp. 770–785, 2013.

[43] K. Tomoda, K. Shingu, M. Osawa, M. Murakawa, and K. Mori, “Comparison of CNS effects of propofol and thiopentone in cats,” *Br. J. Anesth.*, vol. 71, pp. 383–387, 1993.